Geophysical Research Letters

RESEARCH LETTER
10.1029/2023GL104250

Simultaneous Global Ionospheric Disturbances Associated With Penetration Electric Fields During Intense and Minor Solar and Geomagnetic Disturbances

Shun-Rong Zhang[1], Yukitoshi Nishimura[2], Juha Vierinen[3], Larry R. Lyons[4], Delores J. Knipp[5], Björn J. Gustavsson[3], Bhagyashree V. Waghule[5], Philip J. Erickson[1], Anthea J. Coster[1], Ercha Aa[1], and Andres Spicher[3]

[1]Haystack Observatory, Massachusetts Institute of Technology, Westford, MA, USA, [2]Department of Electrical and Computer Engineering and Center for Space Physics, Boston University, Boston, MA, USA, [3]University of Tromsø, Tromsø, Norway, [4]Atmospheric and Oceanic Sciences, University of California, Los Angeles, Los Angeles, CA, USA, [5]Smead Aerospace Engineering Sciences Department, University of Colorado Boulder, Boulder, CO, USA

Abstract A new observational phenomenon, named Simultaneous Global Ionospheric Density Disturbance (SGD), is identified in GNSS total electron content (TEC) data during periods of three typical geospace disturbances: a Coronal Mass Ejection-driven severe disturbance event, a high-speed stream event, and a minor disturbance day with a maximum Kp of 4. SGDs occur frequently on dayside and dawn sectors, with a ~1% TEC increase. Notably, SGDs can occur under minor solar-geomagnetic disturbances. SGDs are likely caused by penetration electric fields (PEFs) of solar-geomagnetic origin, as they are associated with Bz southward, increased auroral AL/AU, and solar wind pressure enhancements. These findings offer new insights into the nature of PEFs and their ionospheric impact while confirming some key earlier results obtained through alternative methods. Importantly, the accessibility of extensive GNSS networks, with at least 6,000 globally distributed receivers for ionospheric research, means that rich PEF information can be acquired, offering researchers numerous opportunities to investigate geospace electrodynamics.

Plain Language Summary Electric fields of solar wind and geomagnetic disturbance origin can penetrate into the low latitude upper atmosphere, influencing the ionospheric dynamics and electron density variations. This study employs a new method that utilizes global and continuous GNSS total electron content (TEC) observations to investigate the electric field effects. The analysis focuses on three geospace disturbance events of different intensities and solar-terrestrial conditions. The study identifies a novel phenomenon named Simultaneous Global Ionospheric Density Disturbance (SGD), primarily occurring on the sunlit portion of the Earth's ionosphere and also near dawn hours with 1% or larger amplitudes of the background TEC, or a few tenths of a TEC unit (10^{16} m^3). The remarkable global extent of ionospheric responses to minor solar-geomagnetic conditions is noteworthy. The solar wind magnetic field directed southward is highly correlated with most SGDs, lasting for up to 30 min. The findings present an effective approach for continuously monitoring electric field penetration and ionospheric impacts, leading to an improved understanding of space weather and its technological implications.

Key Points:

- Simultaneous global ionospheric disturbances (SGDs) are often observed even during minor solar and geomagnetic disturbances
- SGDs occur predominately on dayside and are related to penetration electric fields (PEFs) of solar wind and geomagnetic disturbance origin
- Global GNSS networks offer a novel and effective technique for continuous PEF monitoring, providing rich data sets for further study

Correspondence to:
S.-R. Zhang,
shunrong@mit.edu

Citation:
Zhang, S.-R., Nishimura, Y., Vierinen, J., Lyons, L. R., Knipp, D. J., Gustavsson, B. J., et al. (2023). Simultaneous global ionospheric disturbances associated with penetration electric fields during intense and minor solar and geomagnetic disturbances. *Geophysical Research Letters*, *50*, e2023GL104250. https://doi.org/10.1029/2023GL104250

Received 25 APR 2023
Accepted 17 SEP 2023

Author Contributions:
Conceptualization: Shun-Rong Zhang, Yukitoshi Nishimura, Larry R. Lyons, Philip J. Erickson
Data curation: Shun-Rong Zhang, Yukitoshi Nishimura, Larry R. Lyons, Delores J. Knipp, Bhagyashree V. Waghule, Anthea J. Coster, Andres Spicher
Formal analysis: Shun-Rong Zhang, Yukitoshi Nishimura
Funding acquisition: Shun-Rong Zhang, Yukitoshi Nishimura, Juha Vierinen, Larry R. Lyons, Delores J. Knipp, Philip J. Erickson, Anthea J. Coster

1. Introduction

The Earth's ionosphere is a partially ionized layer of the upper atmosphere that can induce electric fields with diverse spatial and temporal scales, and also be susceptible to the influence of external electric fields from various sources in geospace. The E-region wind dynamo is active during the day as lower thermospheric winds blow plasma across the magnetic field line which is nearly horizontal at equatorial and low latitudes. At midlatitude nighttime, thermospheric winds in the F region height induce the polarization electric field which drives ionospheric dynamics. The high-latitude electric fields have their origin in the solar wind flow across the magnetosphere creating dawn-to-dusk electric fields that are mapped down to ionospheric altitudes. This dawn-to-dusk electric field in the ionosphere varies as a non-linear function of L-value, reaching the magnetic equator at approximately a few tenths mV/m or one-tenth of interplanetary electric field (IEF) (Kelley et al., 2003; Mozer, 1973). This penetration electric field (PEF, Nishida, 1968) has been known to produce significant ionospheric disturbances, especially during intense geomagnetic storms when the large-scale magnetospheric dawn-to-dusk electric fields are severely intensified during the early storm stage to respond to magnetospheric reconnection during

Investigation: Shun-Rong Zhang, Yukitoshi Nishimura, Juha Vierinen, Larry R. Lyons, Delores J. Knipp, Björn J. Gustavsson, Bhagyashree V. Waghule, Ercha Aa, Andres Spicher
Methodology: Shun-Rong Zhang, Yukitoshi Nishimura, Juha Vierinen, Delores J. Knipp, Anthea J. Coster
Project Administration: Shun-Rong Zhang
Resources: Shun-Rong Zhang, Yukitoshi Nishimura, Juha Vierinen, Larry R. Lyons, Delores J. Knipp, Philip J. Erickson, Anthea J. Coster
Software: Shun-Rong Zhang
Supervision: Shun-Rong Zhang
Validation: Shun-Rong Zhang, Yukitoshi Nishimura, Juha Vierinen, Larry R. Lyons, Delores J. Knipp, Björn J. Gustavsson, Bhagyashree V. Waghule, Philip J. Erickson, Anthea J. Coster, Ercha Aa
Visualization: Shun-Rong Zhang, Yukitoshi Nishimura
Writing – original draft: Shun-Rong Zhang
Writing – review & editing: Shun-Rong Zhang, Yukitoshi Nishimura, Juha Vierinen, Larry R. Lyons, Delores J. Knipp, Björn J. Gustavsson, Bhagyashree V. Waghule, Philip J. Erickson, Anthea J. Coster, Ercha Aa

southward turning of the interplanetary magnetic field (IMF) Bz (Fejer et al., 1979; Kelley et al., 2003, 2010). The PEF is also sensitive to variations of auroral electrojets that are caused by solar wind changes and substorms (Kikuchi et al., 1996, 2000). The PEF involves the expanded 2-cell Hall currents as well as Pedersen currents flowing at midlatitudes into the equatorial region where currents are significantly amplified by the Cowling conductivity in the Equatorial electrojet (EEJ) region (Kikuchi et al., 2011; Yizengaw et al., 2016). However, the storm-induced Region-2 field-aligned currents and the ring current can establish the shielding electric field that reduces the magnetospheric electric field penetration into ionospheric lower latitudes (e.g., Vasyliunas, 1970). The long time scale (hours to days) for this shielding electric field can permit the launching of prompt PEF at lower latitudes, although the shielding can sometimes be quick as well (Kikuchi et al., 2010). With Bz northward turning and substorms, the weakening magnetospheric electric field can become unbalanced with the shielding electric fields, and therefore overshielding generates oppositely directed electric fields at mid- and low latitudes (including CEJ, counter EEJ) from the magnetospheric PEF.

Here we broadly define PEF as ionospheric electric fields observed at mid- and low latitudes that could not be explained by either regular wind-driven dynamo electric fields or storm-time disturbance wind dynamo, but appear to be primarily of solar wind-magnetospheric and geomagnetic disturbance origin. Important PEF sources include the IEF change, solar wind dynamical pressure change-related shock front arrival (e.g., Huang, 2020a; Kikuchi et al., 2016), substorm (Fejer & Navarro, 2022), and SubAuroral Polarization Stream (Huang, 2020b) which may appear extended equatorward (Foster & Burke, 2002) and be impacted by auroral streamers (Gallardo-Lacourt et al., 2017). Significant progress has been made in our understanding of the PEF since the 1970s, although some fundamental questions remain highly debatable, for example, what is the physics for the solar wind energy and momentum to be transmitted to the low latitude and equatorial ionosphere (Tu & Song, 2019)? This progress has primarily been made possible by analyzing magnetometer data, which provides crucial information about the electric current, as well as ion drift measurements from some incoherent radars and in situ satellites. PEF impact on the ionosphere and thermosphere can be noted in sophisticated simulations (Lu et al., 2020; K. Zhang et al., 2019a).

The present paper reports GNSS total electron content (TEC) measurements with fine-scale ionospheric perturbations that are most likely caused by PEF. Three sample events were selected representing three different scenarios: a great geomagnetic storm on 17 March 2015, a solar wind high-speed stream event around 14 March 2016, and a Kp 4 event on 6 February 2023. It was found that GNSS TEC in the background-detrended component is very sensitive to PEFs associated with the dynamical solar wind changes, substorm enhancements, and other changes not well understood; these occur globally and simultaneously. The easy accessibility of global GNSS data provides a tremendously rich resource to characterize the PEF, opening up new opportunities to better understand electrodynamics coupling in solar-terrestrial and geospace systems.

2. Observations

MIT Haystack Observatory has been producing global TEC data from over 6,000 receivers contributed by various communities around the world. Currently, these data include observations from both the GPS and GLONASS constellations and TEC is obtained using techniques described in Rideout and Coster (2006) and Vierinen et al. (2016). The TEC data is utilized to further derive ionospheric disturbance information, as represented by differential TEC (dTEC) values, with background TEC variations being detrended (S.-R. Zhang et al., 2017a, 2017b). For this purpose, the background TEC is determined by using a low-pass filter (Savitzky & Golay, 1964) with a linear basis function within a 30-min sliding window (S.-R. Zhang et al., 2019b). These dTEC data have been extensively used in studies related to traveling ionospheric disturbances (TIDs) such as those associated with solar eclipses, solar flares, geospace storms and substorms, volcanic eruptions, and lower atmospheric forcing (Lyons et al., 2019; S.-R. Zhang et al., 2017a, 2017b, 2019b, 2019c, 2022). In the present study, the same detrending technique is employed.

Other data used in this study include solar wind dynamic pressure and IMF Bz (from OMNI, Geotail, and Cluster) and auroral electrojet indices AU and AL. The pressure increases give increases of convection, in addition to IMF changes (Boudaridis et al., 2005; Boudouridis et al., 2004). AU is a measure of convection strength and can respond to a variety of factors, and AL is a measure of substorm activity. Geotail and Cluster are used for the events where they are close to the subsolar bow shock. The propagation time from the satellite location to the bow shock is a few minutes. Since the standard AU and AL indices for the 6 February 2023 event are not yet available,

the equivalent AU and AL indices are calculated by superposing the horizontal component of the high-latitude ground magnetic field variations using data available in International Real-time Magnetic Observatory Network (Intermagnet).

3. Results

Here we present three distinctly different scenarios of simultaneous global ionospheric density disturbances (SGD): *Case* 1, during a severe geomagnetic disturbances on 17 March 2015 (the St Patrick's Day storm; see S.-R. Zhang et al. (2017a, 2017b)). According to Cluster data, the solar wind dynamic pressure reached a ∼12 nPa peak at ∼04:45 UT and Bz reached −29 nT minimum at 14:01 UT. *Case* 2, under the impact of solar wind high speed stream on 14–15 March 2016. Bz reached ∼−20 nT at 18:58 UT (Geotail data) and solar flares B6.4 at 17:58 and B5.1 at 22:45 UT were the strongest during the period of 16:00–04:00 UT on 14–15 March of interest to the study. *Case* 3, during a weak geomagnetic disturbance on 6 February 2023 when the GFZ Potsdam 3-hourly Kp varied between 2 and 4. There were several short episodes of IMF Bz southward turning reaching ∼10 nT. This was also the day of the tragic Turkey earthquakes, however, we do not believe our key results were associated with the earthquakes.

dTEC variations during these periods are shown as keograms in Figures 1–3. The middle panels of each figure demonstrate dTEC variations as a function of UT and longitude for mid- and low latitudes in both hemispheres where more than 30 million data points in each plot were included. These individual data points correspond to original GNSS line-of-sight (LOS) measurements at ionospheric pierce points (without any bin-averaging). The bottom panels show dTEC variation as a function of UT and latitude within 10° longitude span (65–75°W). The most pronounced feature in these dTEC variations is multiple vertically aligned perturbations (increases or decreases) that resemble zebra stripes (bars). These represent almost simultaneous TEC perturbations across the whole dayside ionosphere. For the convenience of further discussion, we number intervals of positive dTEC bars and mark the centers of the preceding *negative* bars with vertical green dashed lines (placed in the top group of panels).

The simultaneous sudden increase or decrease appearing as the zebra stripes is a global phenomenon, particularly at mid- and low latitudes. This latitude span can be seen in the bottom panels of Figures 1–3. At high latitudes, simultaneous increases/decreases are visible (e.g., yellow bars in the south hemisphere in the bottom panel of Figure 2 corresponding to white bars 1–4 above this panel; similarly bars 8–19 in the keograms of Figure 3), despite intense TID activities.

While the longitudinal extent of the zebra bars presents globally, TEC perturbations on the dayside (especially near the dawn sector) are much more prominent. The perturbations on the nightside (especially near the dawn sector) are sometimes visible. There appears a phase reversal (from dTEC increase to decrease) between dayside and nightside; some of the best examples of the change are in Case 1: near bars numbered as 2, 3, 5, 8 in the longitude–UT keogram; their corresponding green arrows in the latitude–UT keogram are located near the dark (negative dTEC) regions. Although the signal is weaker, this can be identified in Case 3 (bar numbers 3, 6, 8–10).

The width of the bars is normally ∼30 min in time and occasionally exceeds ∼60 min corresponding to intense storm conditions. The dTEC amplitude is normally within 0.2 TECu, or ∼1% on average above the background (NB, the bottom panel in Figure 2 shows dTEC in percentage fraction).

To understand these SGDs, we analyze their correlation to solar wind and geomagnetic observations, including IMF Bz, solar wind dynamic pressure, Sym-H index, auroral AU, and AL indices. We use the green lines (determined as the centers of the preceding negative bars) in Figures 1–3) as a approximate reference to the start of dTEC response. As further discussed later, it is reasonable to assume that TEC responses to external forcing (such as PEF) will unlikely cause an impulsive variation in TEC but, as an integral, a gradual change. Indeed almost every dTEC increase (positive) is preceded by a dTEC decrease (negative) or vice versa, although this is partially caused by the de-trending technical nature associated with averaging within a sliding window for dTEC calculation. Triangle marks are also placed at characteristic times where changing conditions in Bz southward, solar wind dynamic pressure sharp increase, and AU and AL enhancements occur. The green lines are near the Bz minimum or drastic changes in the dynamic pressure or Sym-H. Red and blue triangles are for AU and AL respectively (Case 2 does not include blue triangles because the red ones already represent all characteristic times).

10.1029/2023GL104250

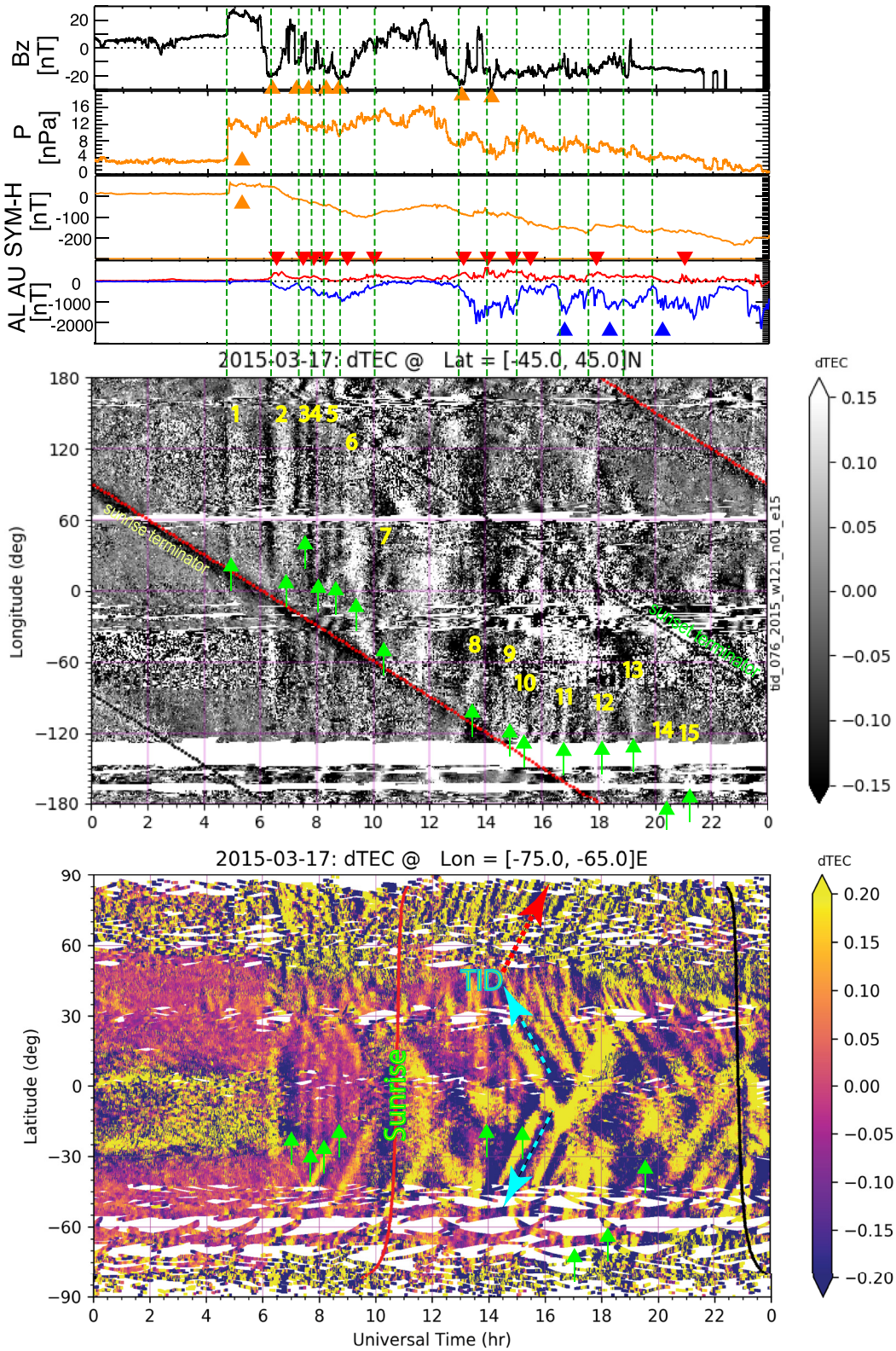

Figure 1.

We can find that the majority of SGD enhancement bars started (as marked by the green lines) at or immediately after Bz southward turning; in Cases 1 and 3, this correlation was higher; In Case 2, the deep negative dTEC bars (e.g., immediately ahead of positive bars 3, 4, 8, 11, and 12) corresponded to Bz northward turning, which caused the decreasing or oppositely directed PEF due to the weakened IEF and overshielding.

We can also find that enhancements of solar wind dynamic pressure are correlated to the SGD enhancement on the dayside (the bar 1 in Case 1 and bar 2 in Case 2). Several SGD bars occurred also during periods of AL drops or AU enhancements when Bz was steadily southward (e.g., bars 10–12, 14, and 15 in Case 1; bright bars 8 and 12 in Case 2). However, identifying the plausible drivers for SGDs becomes less robust when multiple drivers are present almost simultaneously.

4. Discussion

The aforementioned SGD observations are consistent with the PEF-induced ionospheric perturbation effect. This is primarily based on the fact that the simultaneous global presence cannot be explained in terms of neutral winds, composition, and natural day-to-day variability. The solar flares, which would potentially cause similar global dayside impact (see S.-R. Zhang et al. (2019b, 2019c)), did not exist or were too weak during those identified SGD intervals, except for the interval near 12:14 UT in Case 3 when a C7.9 solar flare peaked (according to GOES X-ray 1 min data averaged in 1–8 Å bands). This was the only occasion in the three events where the SGD related dTEC enhancement could be potentially related to a solar flare. See S.-R. Zhang et al. (2019b, 2019c) for more discussions on dTEC responses to solar flares. These SGDs are clearly short-term variability associated with an electric field effect on a global scale. These ionospheric electric fields were highly likely PEFs correlated with the solar wind and geomagnetic field conditions. We can further highlight several important characteristics of dTEC observations associated with PEFs.

The TEC responses are non-impulsive, but show rising/descending phases, suggesting the duration of PEF can last for a while, predominately for ∼30 min. This is consistent with most of the prior PEF results.

The $\mathbf{E} \times \mathbf{B}$ drift associated with zonal PEF has a vertical component. As a result, the F-layer ascending and descending can modify spontaneously the peak height, but not necessarily impose tangible changes in the peak density and TEC. However, if PEF lasts, TEC can increase with the ascending layer because of a combined effect of chemical loss rate change in height and continuous fresh plasma production in time during the day. TEC can decrease with a descending layer due to substantially enhanced chemical loss rates at low heights.

Thus, because of the ionospheric chemical and diffusive effects, TEC and NmF2 tend to low-pass filter the PEF effects. When combined with the fact that the ring current system imposes a high-pass filter to PEF by setting up the shielding electric field, TEC and NmF2 will be a band-pass as a combination of these two filtering effects. This explanation is consistent with the model simulation of NmF2 responses to presumed oscillating Bz with different periods (K. Zhang et al., 2019a). Because of the time lags involved in these filtering processes, however, the instantaneous relationship between TEC and PEF for an individual site may not be always obvious, as further demonstrated in the following discussion of the dTEC time-dependent responses.

Figure 4 presents a group of line plots of TEC observations each along LOS for a given pair of receiver-GNSS. The same IMF Bz (with an understanding that Bz is not the only driver) and the starts (green lines) of SGD intervals (numbered dTEC enhancement bars) as in Figures 1 and 3 are provided for reference. While individual LOS TEC data are normally too complicated to be explained for small fluctuations, *guided by the SGD results* in a global context built from extensive GNSS data, most of the fluctuations may be traced back to Bz changes with some time lags, although it is still challenging to establish a perfect one-to-one correlation. In Case 1, Bz swinging during 06:00–09:00 UT causing nicely organized SGDs (Figure 1) corresponds to clear oscillations in the specific LOS data from a dayside receiver (Figure 4 left): dTEC minimizes and starts to increase following Bz southward turning, and maximizes in a short time. The initial Bz northward increase near 05:00 UT during the storm sudden commencement produced fairly noticeable enhancements in dTEC (see also in Figure 1) and in

Figure 1. Zebra stripe pattern of simultaneous global ionospheric disturbances (SGD) and related solar wind and geomagnetic variations on 17 March 2015 (Case 1). The top group includes interplanetary magnetic field Bz and solar wind dynamic pressure as measured by Cluster C4 (GSM X 10–16 R_E, Y −7 to −6 R_E). The middle panel shows dTEC as a function of UT and longitude over ±45°N latitudes, obtained with 53 million points with a minimum elevation 45°. The bottom panel shows dTEC as a function of UT and latitude over −76 to −65°E longitudes. Other than SGDs, traveling ionospheric disturbances in polar and midlatitude regions were pronounced. SGDs vertical bars are marked by green arrows and numbered (middle panel). Green vertical lines in the top panels represent approximately the start of dTEC responses to characteristic forcing in Bz (orange triangles), dynamic pressure, SYM-H, and AU/AL (red and blue triangles).

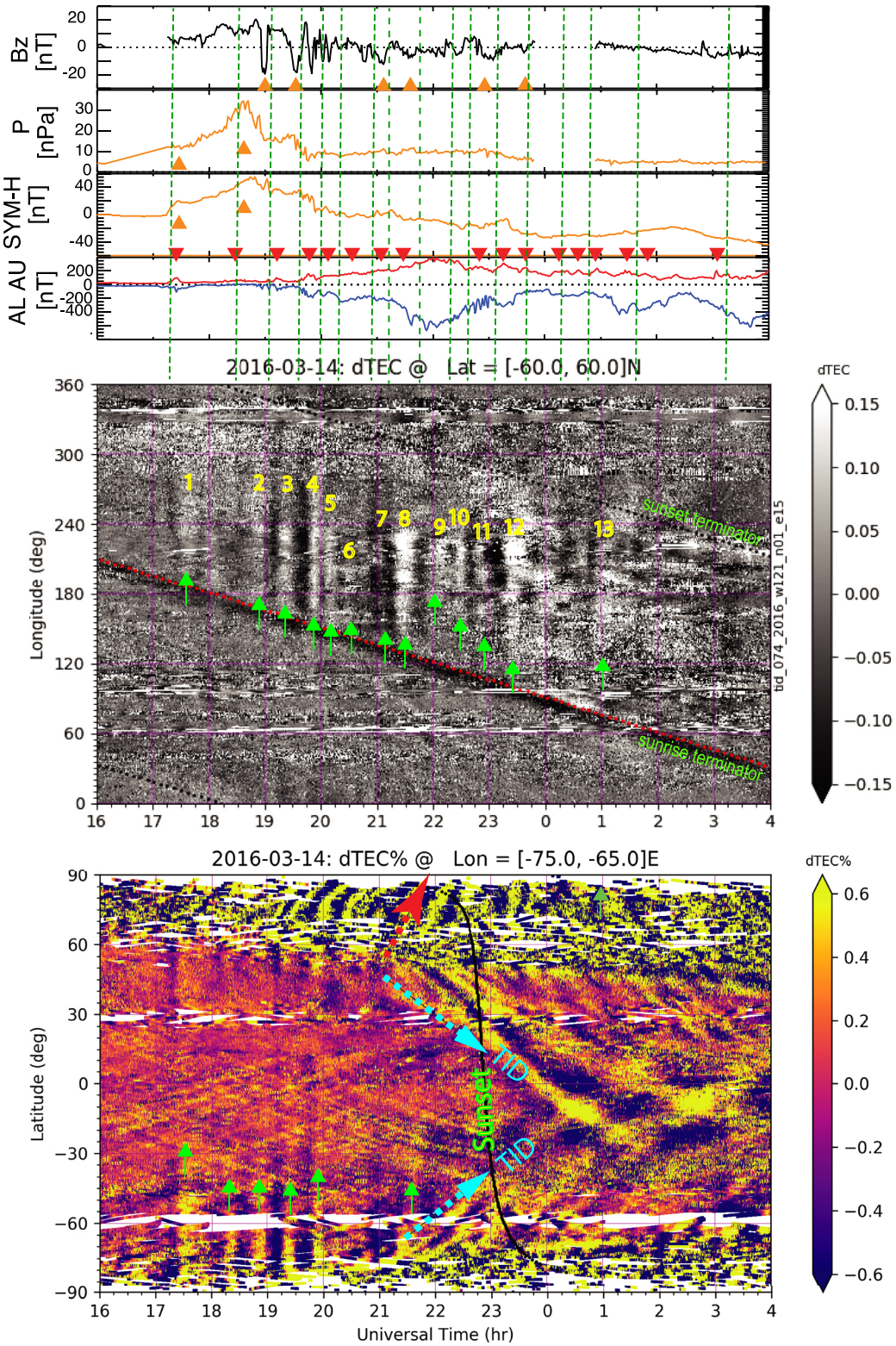

Figure 2. Same as Figure 1 except for the 14 March 2016 (Case 2). The solar wind parameters are measured by Geotail (GSM X 26–29 R_E, Y 3–9 R_E).

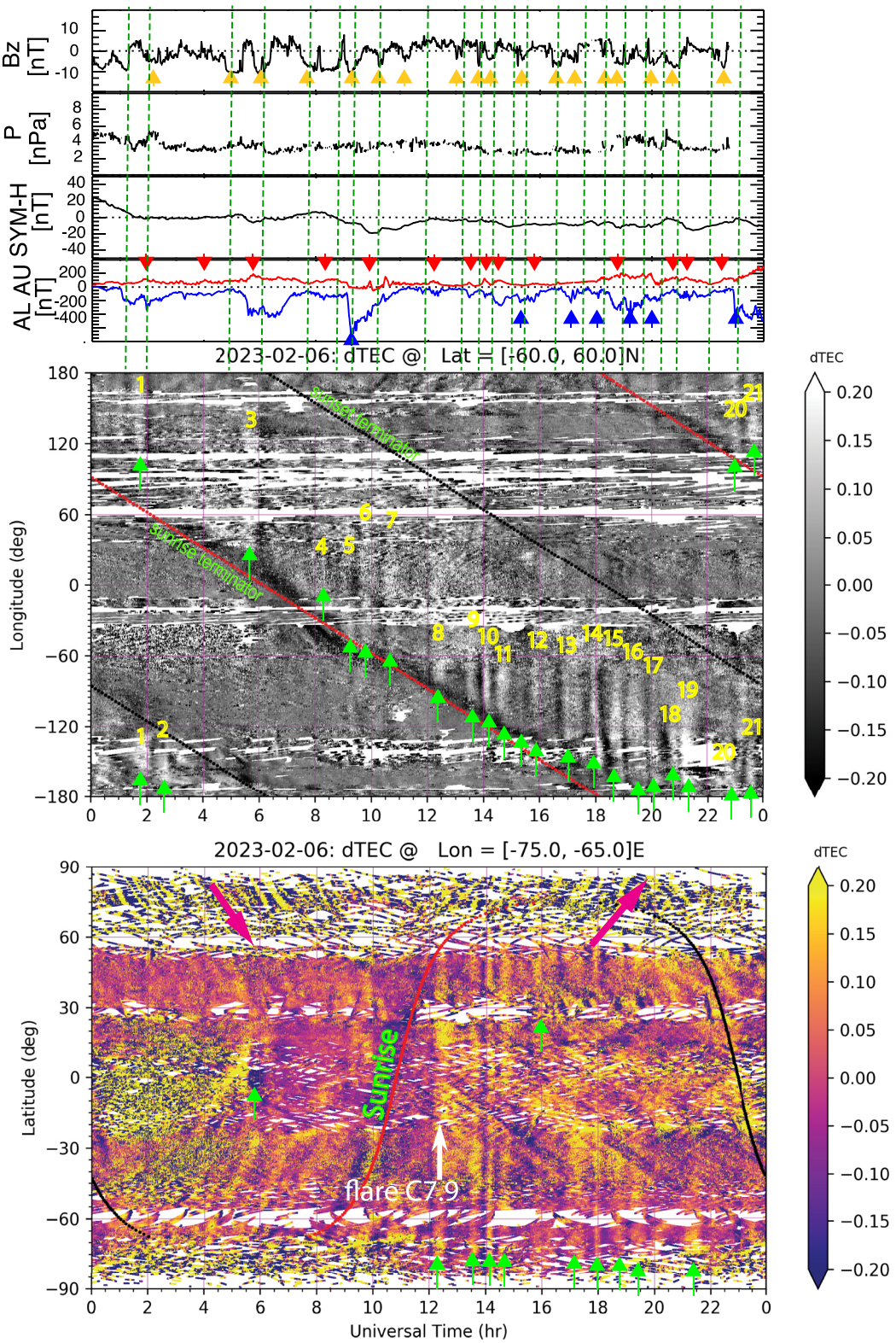

Figure 3. Same as Figure 2 but for 6 February 2023 (Case 3). Solar wind data were from OMIN. A C7.9 solar flare peaked at 12:14 UTC according to GOES X-ray 1 min data averaged in 1–8 Å bands.

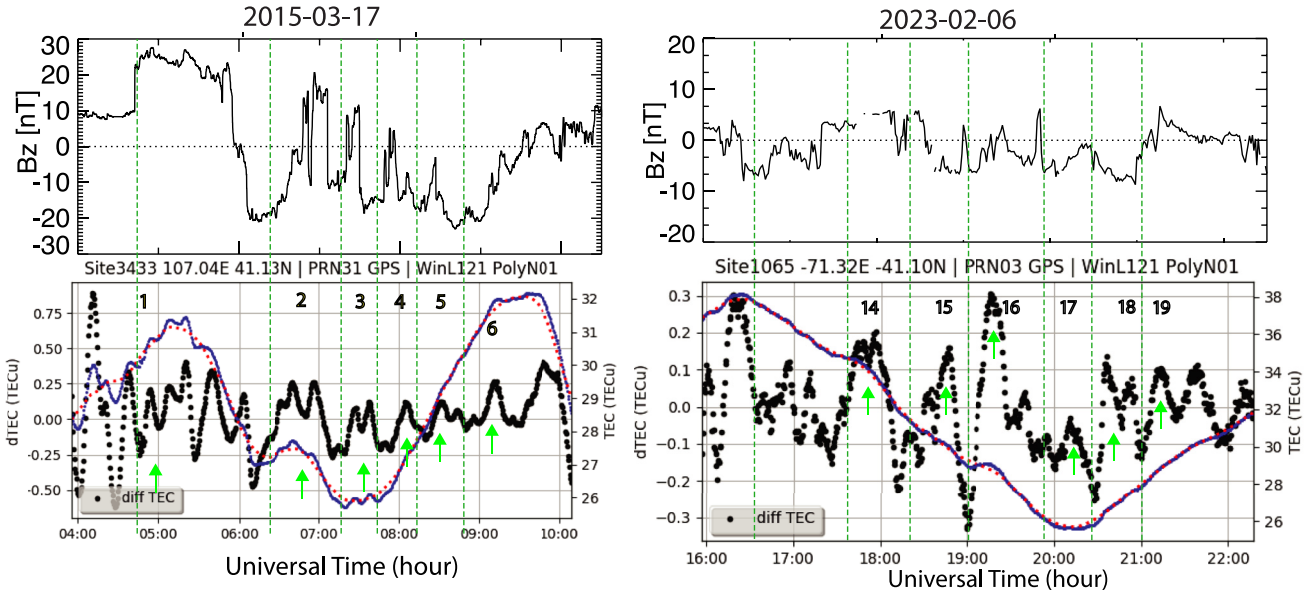

Figure 4. Line plots of pieces of original total electron content (blue in bottom panels) and derived dTEC data (black) with the background variation (red) de-trended using 30-min sliding window (WL121) and linear basis function (PolyN01) to control the Savitzky-Golay filter, solar wind data (top) for Cases 1 and 3. In top panels, vertical lines (green) and numbering of features are the same as in Figures 1 and 3. Please note only solar wind data are repetitively produced here to save space.

original TEC data, maximizing in 30 min, as shown in Figure 4 (left). This is consistent with Kikuchi et al. (2016) that compression of the magnetosphere increases the convection electric field that penetrates to the ionosphere at mid-and low latitudes. Similarly in Case 3, the SGD enhancements at bars 15–18 are correlated with Bz southward turning with small time lags (Figure 4 right). It is worth noting that as the timing marked by green lines to indicate approximately the start of dTEC responses was determined from a very large number of individual data points, individual sites as used in Figure 4 may not always represent the general scenario of dTEC and PEF relationship.

The long-duration (e.g., ≫1 hr) PEF (Huang, 2019) effect on the ionosphere can be difficult to be identified in dTEC. Because the PEF-driven plasma drift can induce thermospheric wind changes due to ion drag, disturbance dynamo effect, thermospheric heating due to frictional heating, and possibly neutral composition changes. Ionospheric responses to these can mask the direct consequence of PEF-driven $\mathbf{E} \times \mathbf{B}$ drift. It should be noted also that our 30-min de-trending method for the dTEC analysis may smooth out, to some extent, long-duration PEF effects. Applying other de-trending techniques to specific types of GNSS data, such as geostationary Beidou data, may enable the resolution of longer-duration PEFs.

The effects of PEF on the ionosphere are widely recognized and comprehended for their manifestation during *severe* geomagnetic storms. Specifically, they cause alterations in the EIA crests, resulting in the formation of the Super Fountain (Mannucci et al., 2005; Tsurutani et al., 2004) and some very pronounced ionospheric responses were reproduced in simulations (Lu et al., 2020). These and other earlier studies (for the Case 1 event, see a summary in S.-R. Zhang et al. (2017a, 2017b) and Kumar and Kumar (2019)) focused typically on few short intervals of intense PEFs using observations at very limited locations. However, it was not clear to what geographic extent those major geomagnetic disturbances and whether some minor solar and geomagnetic disturbances (e.g., Kp < 5) can cause observable global ionospheric impact. The present study provides positive answers to these. Additionally, S.-R. Zhang et al. (2019b) observed the presence of "synchronized differential TEC oscillations" across the continental United States in the aftermath of solar flares on 6, 7, and 10 September 2017, but their source mechanisms were unidentified. It is worth noting that at least during the 6 September event, these oscillations occurred when Bz was steadily southward and AU/AL fluctuated, indicating a possible connection to substorm PEF. During the substorm PEF events reported by Fejer and Navarro (2022) for the 8 September period, SGDs were similarly present in our GNSS data (figures not shown).

Dinsmore et al. (2021) reported a semi-coherent ionospheric pulsing structures (SCIPS) feature in dTEC and the Millstone Hill incoherent scatter radar electron density data. Upon examining dTEC data derived using our dTEC

calculation for their events on 6–8 May 2013 during minor geomagnetic disturbance periods with maximum Kp 3, we identified intervals of SGDs that essentially corresponded to SCIPS. However, we refrain from using the term SCIPS because the dTEC increases we identified as SGDs are not truly impulsive, periodical, nor propagating medium-scale TID-like structures "with a potential origin at high latitudes," as suggested by Dinsmore et al. (2021). Some of those propagating features may be associated with TIDs. The TIDs in all three cases in the present study were trans-equatorial, with Cases 1 and 2 displaying large amplitude TIDs likely triggered in auroral regions; the Case 3 TIDs were not apparently of auroral origin. At high latitudes, TIDs are characterized by trans-polar anti-sunward propagation (Nishimura et al., 2020; S.-R. Zhang et al., 2019c). It is apparent that SGDs were much more easily discernible from a "clear" background ionosphere without severe TID activities.

5. Summary

This study presents the first instances of Simultaneous Global ionospheric Disturbances (SGDs) in TEC observations during nearly 50 intervals of potential PEF events in 3 days. These SGDs occur predominately on the dayside and sometimes on the nightside (especially near the dawn sector) spanning mid- and low latitudes for ∼30 min. It should be noted that these ionospheric observations of SDGs represent PEFs as the net effort of penetration, shielding, and overshielding processes. The majority of the SGDs and the related PEFs were statistically well correlated with Bz southward, which may be at ∼10 nT or weaker, although discernible SGDs occurred responding to Bz northward turning. Moreover, solar wind dynamic pressure and changes in the auroral index AL/AU are frequently in line with the occurrence of SGDs, particularly when the solar wind is stable.

While previous studies have identified various sources of PEFs and ionospheric effects in few regions and time intervals, the most remarkable finding of this study is the simultaneous and distinguishable responses observed globally across a vast number of GNSS observations for many intervals of time. These responses are not limited to intense solar-geomagnetic disturbances but also occur during minor ones with evident southward Bz. These GNSS results offer new insight on short-term ionospheric variability driven by electric fields with the solar-geomagnetic disturbance origin, while also confirming essential findings from previous studies that used alternative methods. The wide accessibility of extensive GNSS TEC observational networks will enable the acquisition of rich PEF information for statistical and case studies (e.g., the critically important spatial distribution and temporal evolution), which can significantly advance our understanding of electrodynamic coupling processes in geospace.

Data Availability Statement

Original line-of-sight TEC data is provided by Madrigal database at http://cedar.openmadrigal.org/; see specific data files (Coster, 2016a, 2016b, 2017, 2023). The solar wind and ground magnetic field data were obtained through https://cdaweb.gsfc.nasa.gov/ and https://imag-data.bgs.ac.uk/.

Acknowledgments
GNSS TEC data processing and Madrigal database system are provided to the community by MIT under NSF Grant (PJE) AGS-1952737 support. This work was supported by NASA Grants (SRZ) 80GSFC22CA011, 80NSSC21K1310, 80NSSC21K1775, (AJC) 80NSSC22K0171, (PJE) 80NSSC22K1013, (NY) 80NSSC18K0657, 80NSSC21K1321, 80NSSC22M0104, (LL) 80NSSC22K0749, 80NSSC22K0323, and (DJK) 80NSSC20K0199; NSF Grants (SRZ) AGS-2033787, AGS-2149698, (NY) AGS-1907698, AGS-2100975, and (BW) AGS-1933040; AFOSR MURI Grant (SRZ, YN, LL, DJK) FA9559-16-1-0364, and ONR Grant (AJC) N00014-17-1-2186 and N00014-23-1-2160. Data for TEC processing is provided from the following organizations: UNAVCO; SOPAC; IGN; IGS; CDDIS; NGS; IBGE; RAMSAC; CORS; Arecibo Observatory, LISN; Topcon; CHAIN; CRS; SONEL; RENAG; GNSS Reference Networks; Finnish Meteorological Institute; and SWEPOS.

References

Boudaridis, A., Zesta, E., Lyons, L., Anderson, P., & Lummerzheim, D. (2005). Enhanced solar wind geoeffectiveness after a sudden increase in dynamic pressure. *Journal of Geophysical Research*, *110*(A5), A05214. https://doi.org/10.1029/2004ja010704

Boudouridis, A., Zesta, E., Lyons, L., Anderson, P., & Lummerzheim, D. (2004). Magnetospheric reconnection driven by solar wind pressure fronts. *Annales Geophysicae*, *22*(4), 1367–1378. https://doi.org/10.5194/angeo-22-1367-2004

Coster, A. (2016a). *GNSS data from the CEDAR madrigal database*. MIT Haystack Observatory. Retrieved from https://w3id.org/cedar?experiment_list=experiments2/2016/gps/14mar16&file_list=los_20160314.001.h5

Coster, A. (2016b). *GNSS data from the CEDAR madrigal database*. MIT Haystack Observatory. Retrieved from https://w3id.org/cedar?experiment_list=experiments2/2016/gps/15mar16&file_list=los_20160315.001.h5

Coster, A. (2017). *GNSS data from the CEDAR madrigal database*. MIT Haystack Observatory. Retrieved from https://w3id.org/cedar?experiment_list=experiments2/2017/gps/17mar17&file_list=los_20170317.001.h5

Coster, A. (2023). *GNSS data from the CEDAR madrigal database*. MIT Haystack Observatory. Retrieved from https://w3id.org/cedar?experiment_list=experiments4/2023/gps/06feb23&file_list=los_20230206.001.h5

Dinsmore, R., Mathews, J., Coster, A., Robinson, R., Sarkhel, S., Erickson, P. J., & Urbina, J. (2021). Multi-instrument observations of SCIPS: 1. ISR and GPS TEC results. *Journal of Atmospheric and Solar-Terrestrial Physics*, *213*, 105515. https://doi.org/10.1016/j.jastp.2020.105515

Fejer, B. G., Gonzales, C., Farley, D., Kelley, M., & Woodman, R. (1979). Equatorial electric fields during magnetically disturbed conditions 1. The effect of the interplanetary magnetic field. *Journal of Geophysical Research*, *84*(A10), 5797–5802. https://doi.org/10.1029/JA084iA10p05797

Fejer, B. G., & Navarro, L. A. (2022). First observations of equatorial ionospheric electric fields driven by storm-time rapidly recurrent magnetospheric substorms. *Journal of Geophysical Research: Space Physics*, *127*(12), e2022JA030940. https://doi.org/10.1029/2022JA030940

Foster, J. C., & Burke, W. J. (2002). SAPS: A new categorization for sub-auroral electric fields. *Eos, Transactions American Geophysical Union*, *83*(36), 393–394. https://doi.org/10.1029/2002eo000289

Gallardo-Lacourt, B., Nishimura, Y., Lyons, L. R., Mishin, E. V., Ruohoniemi, J. M., Donovan, E. F., et al. (2017). Influence of auroral streamers on rapid evolution of ionospheric SAPS flows. *Journal of Geophysical Research: Space Physics*, *122*(12), 12406–12420. https://doi.org/10.1002/2017JA024198

Huang, C.-S. (2019). Long-lasting penetration electric fields during geomagnetic storms: Observations and mechanisms. *Journal of Geophysical Research: Space Physics*, *124*(11), 9640–9664. https://doi.org/10.1029/2019JA026793

Huang, C.-S. (2020a). Systematical analyses of global ionospheric disturbance current systems caused by multiple processes: Penetration electric fields, solar wind pressure impulses, magnetospheric substorms, and ULF waves. *Journal of Geophysical Research: Space Physics*, *125*(9), e2020JA027942. https://doi.org/10.1029/2020JA027942

Huang, C.-S. (2020b). Westward plasma drifts in the nighttime equatorial ionosphere during severe magnetic storms: A new type of penetration electric fields caused by subauroral polarization stream. *Journal of Geophysical Research: Space Physics*, *125*(10), e2020JA028300. https://doi.org/10.1029/2020JA028300

Kelley, M. C., Ilma, R. R., Nicolls, M., Erickson, P., Goncharenko, L., Chau, J. L., et al. (2010). Spectacular low- and mid-latitude electrical fields and neutral winds during a superstorm. *Journal of Atmospheric and Solar-Terrestrial Physics*, *72*(4), 285–291. https://doi.org/10.1016/j.jastp.2008.12.006

Kelley, M. C., Makela, J. J., Chau, J. L., & Nicolls, M. J. (2003). Penetration of the solar wind electric field into the magnetosphere/ionosphere system. *Geophysical Research Letters*, *30*(4), 1158. https://doi.org/10.1029/2002GL016321

Kikuchi, T., Ebihara, Y., Hashimoto, K. K., Kataoka, R., Hori, T., Watari, S., & Nishitani, N. (2010). Penetration of the convection and overshielding electric fields to the equatorial ionosphere during a quasiperiodic DP 2 geomagnetic fluctuation event. *Journal of Geophysical Research*, *115*(A5), A05209. https://doi.org/10.1029/2008JA013948

Kikuchi, T., Hashimoto, K. K., Shinbori, A., Tsuji, Y., & Watari, S.-I. (2011). Penetration of magnetospheric electric fields to the low latitude ionosphere during storm/substorms. In M. A. Abdu & D. Pancheva (Eds.), *Aeronomy of the Earth's atmosphere and ionosphere* (pp. 443–453). Springer Netherlands. https://doi.org/10.1007/978-94-007-0326-1_34

Kikuchi, T., Hashimoto, K. K., Tomizawa, I., Ebihara, Y., Nishimura, Y., Araki, T., et al. (2016). Response of the incompressible ionosphere to the compression of the magnetosphere during the geomagnetic sudden commencements. *Journal of Geophysical Research: Space Physics*, *121*(2), 1536–1556. https://doi.org/10.1002/2015JA022166

Kikuchi, T., Lühr, H., Kitamura, T., Saka, O., & Schlegel, K. (1996). Direct penetration of the polar electric field to the equator during a DP 2 event as detected by the auroral and equatorial magnetometer chains and the eiscat radar. *Journal of Geophysical Research*, *101*(A8), 17161–17173. https://doi.org/10.1029/96JA01299

Kikuchi, T., Lühr, H., Schlegel, K., Tachihara, H., Shinohara, M., & Kitamura, T.-I. (2000). Penetration of auroral electric fields to the equator during a substorm. *Journal of Geophysical Research*, *105*(A10), 23251–23261. https://doi.org/10.1029/2000JA900016

Kumar, S., & Kumar, V. V. (2019). Ionospheric response to the St. Patrick's day space weather events in March 2012, 2013, and 2015 at southern low and middle latitudes. *Journal of Geophysical Research: Space Physics*, *124*(1), 584–602. https://doi.org/10.1029/2018JA025674

Lu, G., Zakharenkova, I., Cherniak, I., & Dang, T. (2020). Large-scale ionospheric disturbances during the 17 March 2015 storm: A model-data comparative study. *Journal of Geophysical Research: Space Physics*, *125*(5), 333. https://doi.org/10.1029/2019ja027726

Lyons, L. R., Nishimura, Y., Zhang, S.-R., Coster, A. J., Bhatt, A., Kendall, E., & Deng, Y. (2019). Identification of auroral zone activity driving large-scale traveling ionospheric disturbances. *Journal of Geophysical Research: Space Physics*, *124*(1), 700–714. https://doi.org/10.1029/2018ja025980

Mannucci, A. J., Tsurutani, B. T., Iijima, B. A., Komjathy, A., Saito, A., Gonzalez, W. D., et al. (2005). Dayside global ionospheric response to the major interplanetary events of October 29–30, 2003 “halloween storms”. *Geophysical Research Letters*, *32*(12), L12S02. https://doi.org/10.1029/2004GL021467

Mozer, F. S. (1973). Electric fields and plasma convection in the plasmasphere. *Reviews of Geophysics*, *11*(3), 755–765. https://doi.org/10.1029/rg011i003p00755

Nishida, A. (1968). Coherence of geomagnetic DP 2 fluctuations with interplanetary magnetic variations. *Journal of Geophysical Research*, *73*(17), 5549–5559. https://doi.org/10.1029/JA073i017p05549

Nishimura, Y., Zhang, S.-R., Lyons, L. R., Deng, Y., Coster, A. J., Moen, J. I., et al. (2020). Source region and propagation of dayside large-scale traveling ionospheric disturbances. *Geophyical Research Letters*, *47*(19), 619. https://doi.org/10.1029/2020gl089451

Rideout, W., & Coster, A. (2006). Automated GPS processing for global total electron content data. *GPS Solutions*, *10*(3), 219–228. https://doi.org/10.1007/s10291-006-0029-5

Savitzky, A., & Golay, M. J. E. (1964). Smoothing and differentiation of data by simplified least squares procedures. *Analytical Chemistry*, *36*(8), 1627–1639. https://doi.org/10.1021/ac60214a047

Tsurutani, B., Mannucci, A., Iijima, B., Abdu, M. A., Sobral, J. H. A., Gonzalez, W., & Vasyliunas, V. M. (2004). Global dayside ionospheric uplift and enhancement associated with interplanetary electric fields. *Journal of Geophysical Research*, *109*(A8), A08302. https://doi.org/10.1029/2003JA010342

Tu, J., & Song, P. (2019). On the momentum transfer from polar to equatorial ionosphere. *Journal of Geophysical Research: Space Physics*, *124*(7), 6064–6073. https://doi.org/10.1029/2019JA026760

Vasyliunas, V. (1970). *Mathematical models of magnetospheric convection and its coupling to the ionosphere, particles and fields in the magnetosphere b* (Vol. 60). BM McCormac.

Vierinen, J., Coster, A. J., Rideout, W. C., Erickson, P. J., & Norberg, J. (2016). Statistical framework for estimating GNSS bias. *Atmospheric Measurement Techniques*, *9*(3), 1303–1312. https://doi.org/10.5194/amt-9-1303-2016

Yizengaw, E., Moldwin, M. B., Zesta, E., Magoun, M., Pradipta, R., Biouele, C. M., et al. (2016). Response of the equatorial ionosphere to the geomagnetic DP 2 current system. *Geophysical Research Letters*, *43*(14), 7364–7372. https://doi.org/10.1002/2016GL070090

Zhang, K., Liu, J., Wang, W., & Wang, H. (2019a). The effects of IMF Bz periodic oscillations on thermospheric meridional winds. *Journal of Geophysical Research: Space Physics*, *124*(7), 5800–5815. https://doi.org/10.1029/2019JA026527

Zhang, S.-R., Coster, A. J., Erickson, P. J., Goncharenko, L. P., Rideout, W., & Vierinen, J. (2019b). Traveling ionospheric disturbances and ionospheric perturbations associated with solar flares in September 2017. *Journal of Geophysical Research: Space Physics*, *60*(8), 895. https://doi.org/10.1029/2019JA026585

Zhang, S.-R., Erickson, P. J., Coster, A. J., Rideout, W., Vierinen, J., Jonah, O., & Goncharenko, L. P. (2019c). Subauroral and polar traveling ionospheric disturbances during the 7-9 September 2017 storms. *Space Weather*, *17*(12), 1748–1764. https://doi.org/10.1029/2019sw002325

Zhang, S.-R., Erickson, P. J., Goncharenko, L. P., Coster, A. J., Rideout, W., & Vierinen, J. (2017a). Ionospheric bow waves and perturbations induced by the 21 August 2017 solar eclipse. *Geophyical Research Letters*, *44*(24), 12067–12073. https://doi.org/10.1002/2017gl076054

Zhang, S.-R., Vierinen, J., Aa, E., Goncharenko, L. P., Erickson, P. J., Rideout, W., et al. (2022). 2022 Tonga volcanic eruption induced global propagation of ionospheric disturbances via lamb waves. *Frontiers in Astronomy and Space Sciences*, *9*, 871275. https://doi.org/10.3389/fspas.2022.871275

Zhang, S.-R., Zhang, Y., Wang, W., & Verkhoglyadova, O. P. (2017b). Geospace system responses to the St. Patrick's Day storms in 2013 and 2015. *Journal of Geophysical Research: Space Physics*, *122*(6), 6901–6906. https://doi.org/10.1002/2017ja024232